



Densification, microstructure and properties of mechanically alloyed and hot-pressed Cu–15 wt% Al alloy

Mahammad Ali Shaik¹ and Brahma Raju Golla^{1,*}

¹ Metallurgical and Materials Engineering Department, National Institute of Technology, Warangal 506 004, India

Received: 2 April 2018

Accepted: 20 June 2018

Published online:
28 June 2018

© Springer Science+Business
Media, LLC, part of Springer
Nature 2018

ABSTRACT

In the present work, hot press of Cu–15 wt% Al alloys was carried out in a vacuum environment at a sintering temperature of 500 °C for 30 min with varying pressure (100–500 MPa) to densify the alloys. Both the density and hardness of Cu alloys were significantly increased with increasing the hot press pressure. A maximum density of $\sim 94.5\%$ pth (theoretical density) and microhardness of ~ 6.2 GPa was achieved for Cu–Al alloy after hot press at 500 °C with 500 MPa pressure application. The XRD, SEM-EDS analysis confirms the presence of solid solution α ($\text{Cu}_{0.78}\text{Al}_{0.22}$) and γ (Cu_9Al_4) intermetallic phases in the sintered samples. Maximum hardness of 7.88 GPa and elastic modulus of 177.35 GPa was measured for Cu–Al alloy using nano-indentation test. It must be noted that so far in the literature a maximum hardness of 4.9 GPa was reported for Cu-based materials. The alloy was also measured with a moderately high compressive yield strength (1019 MPa), compressive strength (1106 MPa), and a reasonable amount of strain (6.6%). The wear tests revealed that the Cu–15 Al alloy hot pressed at 500 MPa pressure can exhibit better wear properties. Low coefficient of friction (COF) of 0.15 and wear rate of $0.71 \times 10^{-5} \text{ mm}^3/\text{N}\cdot\text{m}$ was observed at a sliding speed of 0.25 m/s and high COF of 0.20 and wear rate of $4.33 \times 10^{-5} \text{ mm}^3/\text{N}\cdot\text{m}$ were noted with further increasing the sliding speed (1.25 m/s). Further microstructural characterization of worn surfaces reveals abrasion wear as the major dominant wear mechanism. The present work clearly demonstrates the use of a high amount of hot press pressure in achieving good sinter density for Cu–15 wt% Al alloys with superior hardness, better wear and compressive strength properties.

Address correspondence to E-mail: gbraju121@gmail.com; gbraju@nitw.ac.in

Introduction

Cu alloys have the potentiality for various applications such as bearings, welding electrodes, rocket nozzle, heat sink, combustion chamber, aircraft, automotive, naval engineering and electrical applications due to its excellent wear resistance, electrical and thermal conductivity, strength and corrosion resistance [1–4]. Cu has been alloyed with different alloying elements such as Al, Fe, Zn, Sn, W, Zr and Cr to further enhance its properties [1–19]. In all these cases, the properties of Cu alloys were enhanced by either solid solution strengthening or precipitation hardening or refining the grain size by a combination of mechanical working and heat treatment. Different fabrication techniques such as casting [5], forging [7], mechanical alloying [6], powder metallurgy [8], high-pressure torsion [10], [11], severe plastic deformation and cryo-rolling [12] have been used to produce Cu-based alloys or composites. Among these processing methods, powder metallurgy (PM) is found to be the one of the promising technique for making homogeneous Cu alloys even with incorporating a large amount of alloying elements, with fine (ultra-fine or nano) microstructure and improved properties [13].

Commercially Cu–Al alloys are popularly known as Cu–Al bronzes or Al bronzes and are of particular interest for marine and automobile applications due to its excellent wear, corrosion resistance and good mechanical properties [1–3]. In particular, Cu–Al alloys are available with various amounts of aluminium addition (up to 10 wt%) [15]. Krebs et al. [1] investigated the use of Cu–10Al–5Fe–5Ni as a coating material to reduce cavitation damage of ship rudder. It has to be noted that generally other alloying elements such as Fe, Ni, Si, Mg were added to Cu–Al alloys for improving specific properties [5]. In another work, Meyer et al. [2] reported that Cu–Al bronze as non-sparking material since no mechanical sparks occurred when the bronze was in contact with stainless steel. Gyimah [3] recently developed new Cu–Al-based composite material for train brake pad application and it was stated that materials processed at a high sintering temperature of 950 °C exhibited high wear properties in view of its better density. Soliman and Habib [4] observed that ageing (at 450 °C for 12 h) of Cu–12.5 wt% Al shape memory alloy doubled the hardness ($262 H_v$) when compared to unaged alloy.

In recent years, researchers paid more attention towards the mechanical alloying of Cu-based alloys due to its potential and versatility in producing alloys, and nanocrystalline materials with improved properties [20–23]. Youssef et al. [20] reported the effect of grain size on mechanical and electrical properties of bulk nanocrystalline Cu–1at.% Nb alloy prepared by mechanical alloying. High yield strength of 1035 MPa was reported for Cu–1at.% Nb alloys and it was attributed to its fine grain structure (~ 18 nm). In another work, the saturation limit of solubility in Cu–Fe system was significantly enhanced by the mechanical alloying approach [21]. Also, the ball milling procedure was adopted to enhance the solid solubility of Cu–Cr–Mo ternary system [22]. As the milling time increased up to 50 h, the particle size of Cu–20Cr(Mo) alloy considerably reduced to less than 20 nm. Further, these nano-sized powders enhanced the densification of the Cu alloy [22]. Chakravarty et al. explained the grain size stabilization and strengthening of cryomilled nano-Cu–12at.%Al alloy [23]. It was demonstrated that the hardness of the nano-sized alloy was significantly increased when compared to raw powders.

As far as the novelty of the work is concerned, most commonly Cu is alloyed with Al up to 10 wt% and studies with more amount of Al use were very much limited in the literature. Detailed microstructural characterization has been carried out using X-ray diffraction (XRD) and scanning electron microscopy with energy-dispersive spectroscopy (SEM–EDS). Hardness behaviour, compression and wear properties of Cu–15Al alloy were studied in detail. The present work explores whether high amount of Al addition (15 wt%) has any beneficial effects on Cu. Also an attempt was made to understand whether Cu–Al alloys can be densified at a low sintering temperature by applying a higher amount of hot press pressure (up to 500 MPa). It has three implications: (1) achieving good density at low sintering temperature can result in improvement in properties due to fine structure, (2) avoiding use of multiple combinations of processes, for example, most of the instances heat treatment is used as additional step with the primary process in order to improve properties, and (3) reducing the processing cost considerably.

Experimental procedure

Processing of Cu–Al alloy

In this work, highly pure commercial powders of copper (99.5% purity, mean particle size $\sim 9.98 \mu\text{m}$, Padmasree enterprises, Hyderabad, India) and aluminium (99% purity, mean particle size $\sim 6.47 \mu\text{m}$, SRLTM) in appropriate proportion were ball milled to prepare Cu–15 wt% Al alloy. The powders were wet ball milled using planetary ball mill at 260 rpm for 10 h and powder to ball ratio was kept at 1:10. The elemental powders were loaded in stainless steel (SS) vials with stainless steel balls and toluene as a dispersing media. After milling, toluene was separated from the Cu–Al powders by the process of evaporation using the rotary vacuum evaporator and the powders were dried at 98 °C for 30 min. The consolidation of Cu–Al alloy was carried out using the hot press at a sintering temperature of 500 °C for 30 min in vacuum (1.3×10^{-2} mbar) environment with application of pressure (100, 300 and 500 MPa). The hot press experiments were performed with a heating rate of 10 °C/min. The hot-pressed discs were of 15 mm in diameter and 4–5 mm in height. The bulk density of the Cu–Al alloys was measured by the Archimedes method (using distilled water as an immersion medium).

Microstructural characterization and mechanical properties evaluation

The phase evaluation of starting materials, ball-milled powders and the sintered samples was done using a pan analytical X-ray diffraction (XRD) equipment (Model: XPERT Pro) using Cu–K α radiation ($\lambda = 1.5405 \text{ \AA}$). Further, the microstructural characterization of the alloys was carried out using scanning electron microscopy (SEM) (TESCAN VEGA 3 LMU) equipped with energy-dispersive spectroscopy (EDS) detector from Oxford instruments. The hardness of samples was measured using Vickers microhardness tester (Shimadzu, HMV). Initially, the Vickers hardness of samples was measured at a load of 100 g for 30 s. It has to be noted here more detailed mechanical properties evaluation (nano-indentation and compression tests) was carried out for the sample that exhibited maximum hardness (i.e. the sample hot pressed at temperature: 500 °C, pressure: 500 MPa, time: 30 min). The effect of load on Vickers hardness of samples was studied at load ranging

from 10 to 2000 g for 30 s. Nano-indentation test (Model: Nano Test Ventage, Microsoft Materials, UK) was also performed to assess indentation and mechanical behaviour of the materials. Berkovich indenter with a curvature radius of 150 nm was selected to find the hardness and elastic modulus. The test was carried out at a constant peak load of 20 mN with loading and unloading rate of 2.0 mN/s. A total of 100 indentations (pattern of 10×10 sized matrix with 40- μm spacing) were made on various locations of the surface under same conditions. The compression test of hot-pressed alloys was conducted on the universal testing machine (UTM) (Instron, Model No: 5982, USA) at a strain rate of 0.02 mm/min. Cylindrical samples of 10 mm diameter (d) and 15 mm length (l) with l/d ratio of 1.5 was used for conducting compression test. A minimum of three measurements were taken for the compression test. The fractography of compression test samples was carried out by means of SEM.

Pin-on-disc wear test

Wear test was conducted on the pin-on-disc wear testing machine (Model: TR-20, Ducom, Bangalore). The Cu–15Al alloy samples with the size of 10 mm in diameter and 15 mm in height were manually polished with 2000 grit-sized silicon carbide paper; further, the samples were fine polished with diamond abrasive and the samples were ultrasonically cleaned. The sample surface roughness (R_a) was maintained to 0.15 μm . According to wear test standard (ASTM G99), the sample's surface arithmetic average roughness $\leq 0.8 \mu\text{m}$ is usually recommended. In the literature, normally for conducting wear tests of Cu, samples are prepared with good surface finish ($R_a \sim 0.20 \mu\text{m}$) [24]. The roughness of wear samples was measured by Taylor Hobson digital surface roughness tester (model: surtronic S-100). Three readings for surface roughness were taken and the average values are presented.

Stainless steel (En31 Grade, HRC 60) disc was used as a counter body to conduct wear tests. The pin-on-disc wear test was conducted according to ASTM G99 standard in dry sliding conditions under 9.81 N load at a sliding velocity (low sliding velocity of 0.25 m s^{-1} for 30 min with a sliding distance up to 450 m and a high sliding velocity of 1.5 m s^{-1} for 27 min with a sliding distance up to 2500 m.) of 0.25 and 1.5 m s^{-1} . The wear test was conducted under similar conditions on three samples, and their average

frictional coefficient, weight loss, wear volume and specific wear rate were evaluated. The microstructure of worn surfaces was observed using SEM-EDS.

Results and discussion

Densification and microstructural characterization

The morphology and X-ray diffraction patterns of starting elemental powders are shown in Fig. 1. The copper powders appeared to be in spherical form,

and aluminium was in the mixed form with combination of semi-spherical and elongated rod shape particles. The corresponding XRD patterns show the peaks having (hkl) values of (111), (200), (220), (311), (222) and (440) for pure copper and aluminium (Fig. 1c, d). Figure 2a, b presents the XRD of ball-milled powders and hot-pressed Cu–15Al samples. After ball milling, the XRD analysis of Cu–Al powders revealed the presence of copper-rich α solid solution ($\text{Cu}_{0.92}\text{Al}_{0.08}$). Its crystal structure is FCC and has lattice parameter (a) equal to 0.3634 nm and the minor γ (Cu_9Al_4) phase is having a cubic crystal

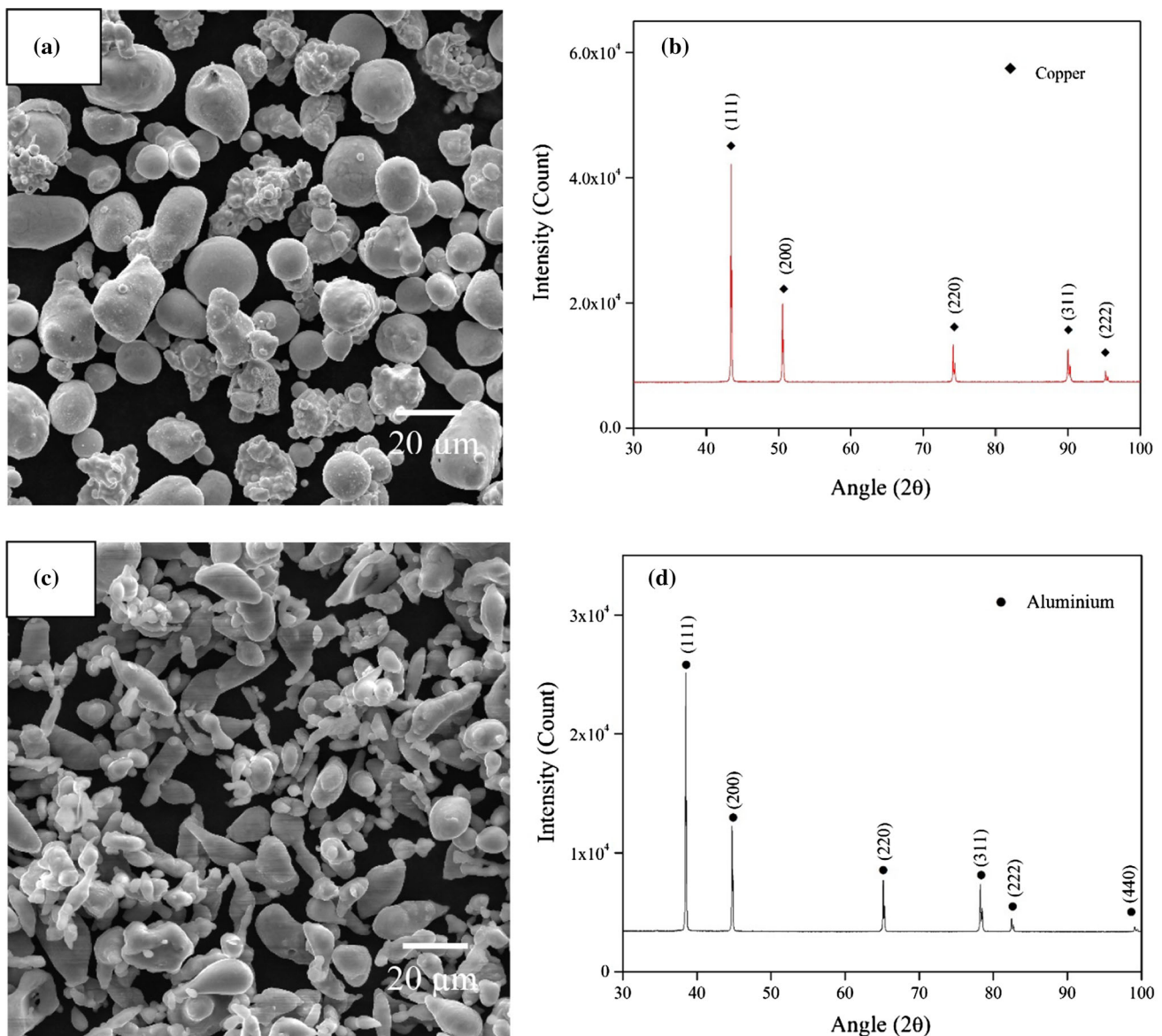


Figure 1 SEM and XRD diffraction patterns of starting elemental powders of **a, b** copper having a mean particle size of $\sim 9.98 \mu\text{m}$ and **c, d** aluminium having a mean particle size of $\sim 6.47 \mu\text{m}$.

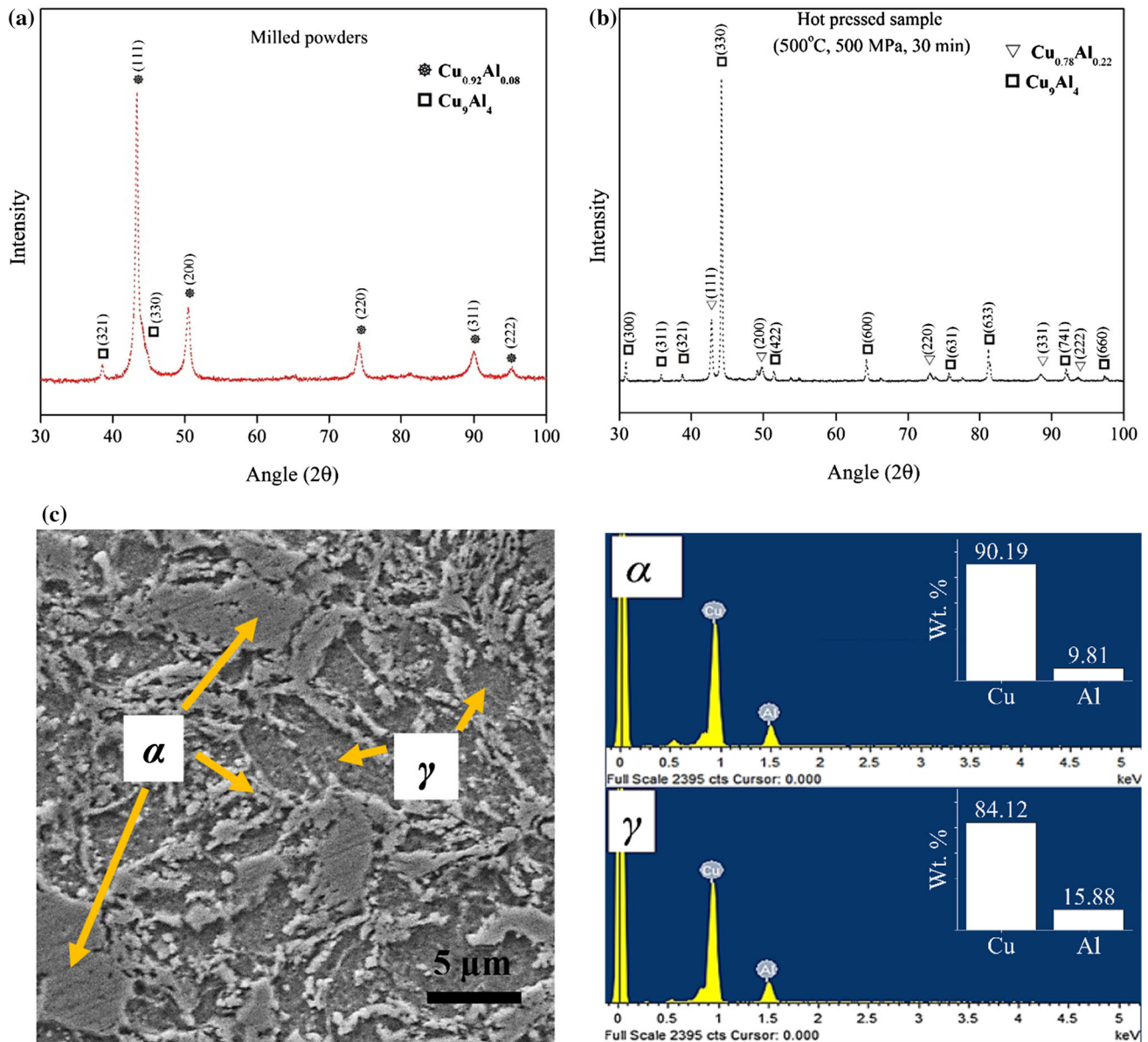


Figure 2 X-ray diffraction patterns of **a** Cu–15Al ball-milled powders, **b** the hot-pressed sample and **c** SEM image of etched Cu–15Al. The hot press is carried at 500 °C, 500 MPa, 30 min under vacuum. The microstructure consists of different contrasting

structure with P-43 m space group ($a = 0.87$ nm). On the other hand, the XRD of hot-pressed samples consists of α solid solution ($\text{Cu}_{0.78}\text{Al}_{0.22}$) as minor phase, whose crystal structure is FCC ($a = 0.367$ nm) and γ (Cu_9Al_4) as a major phase. By using the Bragg's law, the lattice parameter of α ($\text{Cu}_{0.78}\text{Al}_{0.22}$) phase at its major peak was calculated to be 0.361 nm and for γ phase, it was of 0.8685 nm. These calculated lattice parameter values were in good agreement with the JCPDS values and thus complements the presence of

phases, α phase: $\text{Cu}_{0.78}\text{Al}_{0.22}$ and γ phase: Cu_9Al_4 . The respective EDS of the phases is also shown in the figure. The average grain size (bigger grains) of α phase is 7.83 μm and γ phase it is of 5.51 μm .

α ($\text{Cu}_{0.78}\text{Al}_{0.22}$) and γ phases in the hot-pressed alloy. From the XRD, based on the relative intensity of different phases, the amount of α ($\text{Cu}_{0.78}\text{Al}_{0.22}$) phase was estimated to be 28.3 vol% and the balance (71.7 vol%) as the γ phase. The SEM image of polished and etched Cu–Al alloy also clearly showed the presence of two contrasting phases (see Fig. 2c). The SEM-EDS analysis of α ($\text{Cu}_{0.78}\text{Al}_{0.22}$) phase consisted with copper content of 90.2 wt% and aluminium of 9.8 wt%, whereas the γ (Cu_9Al_4) phase consisted of copper

content of 84.1 wt% and aluminium of 15.9 wt%. The morphology of α and γ phases appeared to be very irregular in shape and varying in size as well. The average grain size (coarser grains) of α phase was estimated to be about 7.83 μm and coarser grain size of γ phase was about 5.51 μm .

The density of Cu–15Al as a function of hot press pressure after sintering at 500 °C for 30 min is shown in Fig. 3a. The experimental density of sample increased from 6.0 to 6.61 g/cc with increasing the hot press pressure from 100 to 500 MPa. It indicates that the relative density of samples increased considerably from 86.1 to 94.5% of its theoretical density ($\rho_{\text{th}} \sim 6.99$ g/cc) with pressure. It has to be noted

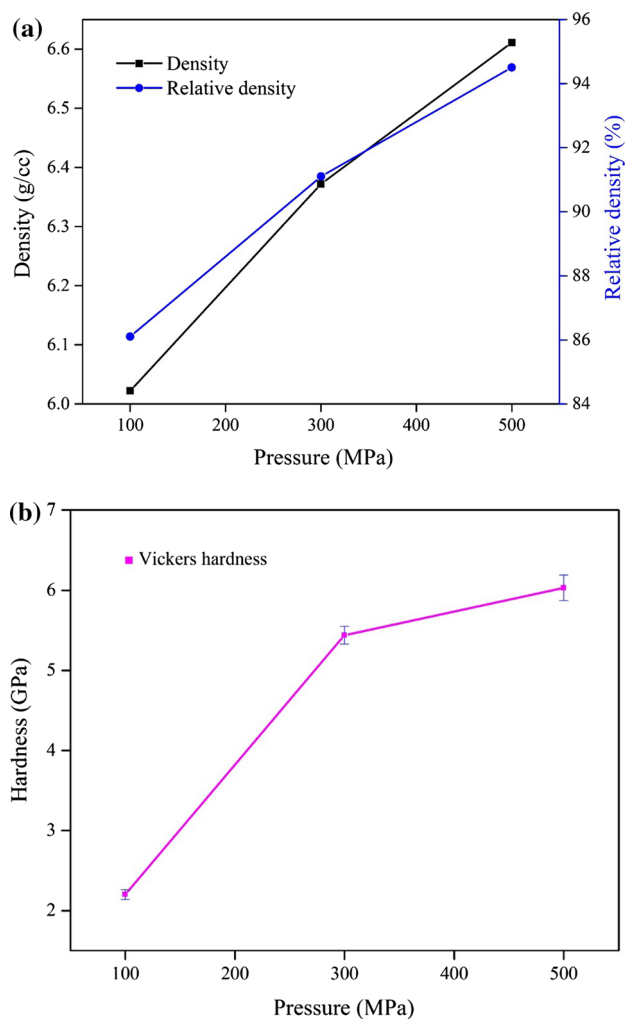


Figure 3 Effect of hot press pressure on **a** density and **b** Vickers hardness of Cu–15Al after sintering at 500 °C for 30 min under vacuum. (The hardness was measured at 100 g load with a dwell time of 30 s).

that the theoretical density of samples was estimated by Rietveld analysis of XRD patterns using X'Pert highscore software. The densities of $\text{Cu}_{0.78}\text{Al}_{0.22}$ [14] and Cu_9Al_4 [15] phases were taken as 7.46 and 6.84 g/cc, respectively, for theoretical density calculation. Han et al. [16] studied the effect of hot press conditions on densification and mechanical properties of Cu–25Sn alloy. The hot press of Cu–Sn alloy was carried by varying temperature (421–600 °C) at a pressure of 25 MPa for 4 min. The relative density of Cu–Sn alloy reportedly varied in the range of 88.4–90.7% depending on hot press conditions. Such low density can be attributed to the use of very short sintering time. Rojas et al. [17] processed Cu–50Ni and Cu–40Ni via hot press at 300 °C under 900 MPa pressure for 5 h. They could achieve a maximum relative density of 78%. In this case, the low sintering temperature should have resulted in poor densification. In another work, Martínez et al. [18] studied microstructure and mechanical properties of hot-pressed Cu-based systems such as Cu–Ni, Cu–Zr and Cu–Ni–Zr alloys. These alloys were processed at a hot press temperature of 300 °C and pressure of 900 MPa. The low relative density of 78, 74 and 72% was reported for Cu–50Ni, Cu–50Zr and Cu–10Ni–40Zr alloys, respectively. The maximum density of 97.5% was achieved for mechanically alloyed Cu–10Zn after hot press at a high temperature of 900 °C, pressure of 25 MPa for 1 h [19]. Sharma et al. [25] reported a maximum of 90% ρ_{th} for Cu–10 Pb alloy even with the use of advanced sintering technique such as SPS (spark plasma sintering) at 350 °C with the application of 100 MPa. In another work, SPS-processed Cu–10 TiB₂ composites could be densified to 72% ρ_{th} at 400 °C under 50 MPa for a holding time of 5 min and with further increasing temperature up to 700 °C they could only achieve a maximum of 91% ρ_{th} [26]. Eze et al. [27] could achieve maximum densification of 96.3% for Cu–1wt% Ti with SPS (650 °C, 50 MPa, 5 min). By controlling sintering temperature (600 °C) and sintering time (148 s), almost full density was achieved for pure Cu powders using novel micro-fast (field-activated sintering technology) [28]. Plastic deformation and interfacial melting of powders were attributed to the enhancement of density. Patra et al. [29] observed that with increasing cold compaction pressure (up to 600 MPa) and high sintering temperature (1000 °C) for 30 min resulted in maximum densification of $\sim 93\%$ in conventional sintered Cu–8 at.% Cr. In a different

work, Kumar et al. [30] studied the effect of mechanical alloying and sintering conditions on densification of Cu–20Mo. They achieved maximum density of 92.3% after sintering at 1000 °C for 1 h. It was reported that small amount (0.5 wt%) of elements such as Cr, Ti, Al aid in densifying (> 90%) Cu at 950 °C for 2 h as these elements can remove surface oxides of Cu and promote densification, while Mo, Nb and W impede densification of Cu [30]. From this, it can be realized that optimal sintering conditions are needed to achieve a higher density of Cu-based materials.

In the present work, achieving higher density of 94.5% ρ_{th} for Cu–15 Al alloy at a lower hot press temperature of 500 °C is a promising result. As far as the densification mechanisms are concerned, mechanical alloying (lattice strains, crystallite size reduction and defect structure) and use of high hot press pressure (a large amount of plastic deformation, particle rearrangement and an increase of contact area between particles) should have aided the densification of Cu–15Al alloy.

Mechanical properties

Vickers microhardness

Figure 3b shows that the Vickers hardness of Cu–15Al sample significantly improved from 2.10 to 6.16 GPa with increasing hot press pressure. The improvement in hardness can be attributed to the enhancement of densification with hot press pressure. At low hot press pressure of 100 MPa, the internal porosity (13.9%) possessed by Cu–15Al alloy resulted in the low hardness value of 2.1 GPa. On the other hand, as hot press pressure increased from 300 to 500 MPa, the porosity of the Cu–15Al alloy decreased from 8.9 to 5.5%. As a result, its hardness increased from 5.44 to 6.16 GPa. So far in the literature for Cu-based materials a maximum hardness of 4.1 GPa was reported [8, 17–19, 25–35]. In case of hot-pressed Cu–10 Sn alloys, the hardness varied between 1.12 and 2.46 GPa [32]. In particular, for Cu–Al alloys, a maximum of 3.7 GPa was measured by Glas [36]. These results clearly indicate that Cu–15Al alloy is exhibiting superior hardness when compared to the literature results.

Hardness behaviour of Cu–15Al sample (hot pressed at 500 MPa) was further explored as it

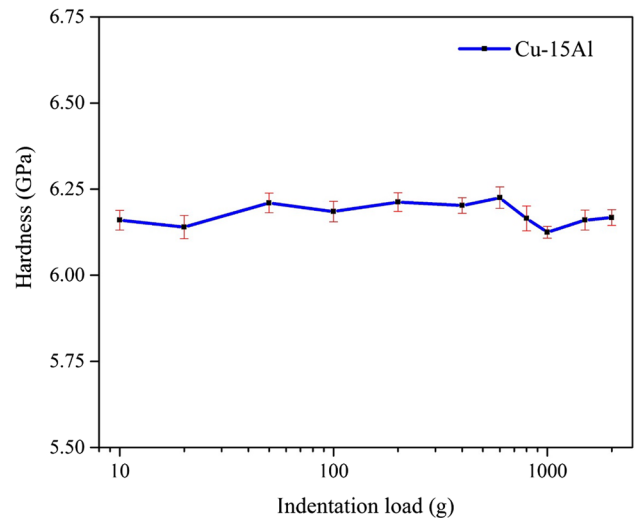
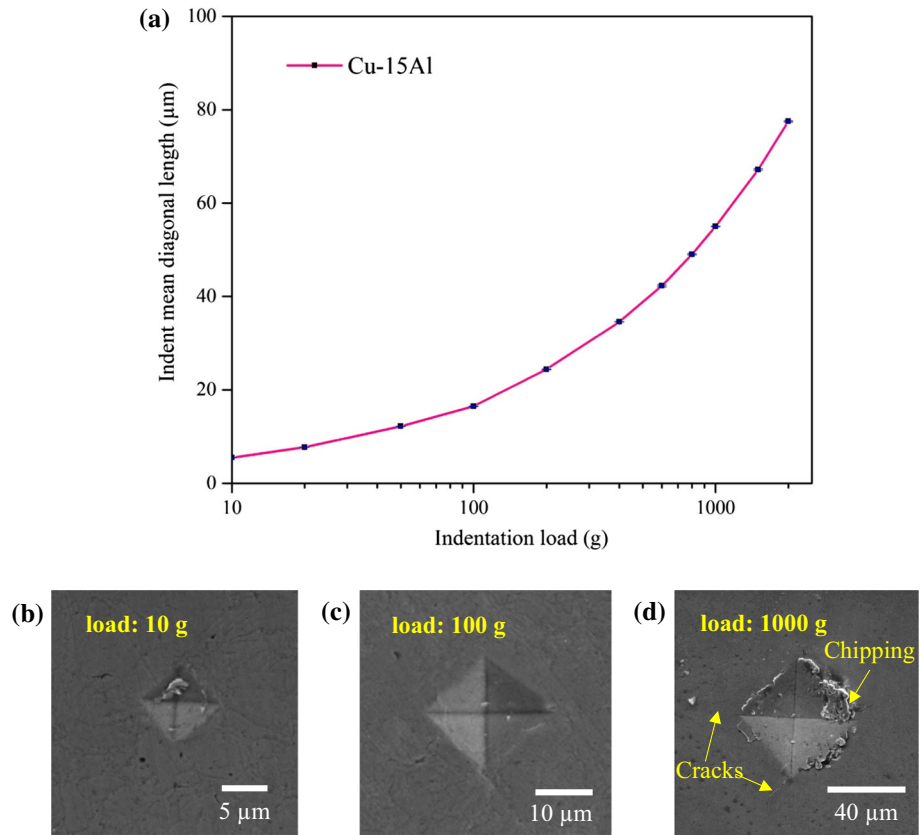


Figure 4 Effect of indentation load (range: 10–2000 g) on Vickers hardness of Cu–15Al sample after hot press at 500 °C, 500 MPa for 30 min.

exhibited relatively higher hardness. The effect of indentation load on microhardness of Cu–Al is presented in Fig. 4. The average hardness of alloy is varying in the range between 6.12 ± 1.7 and 6.21 ± 2.6 GPa with respect to change in indentation load. The average hardness of Cu–15Al remains almost same over the applied load ranging between 10 and 2000 g. A close look at Fig. 4 reveals a slight reduction in the hardness at above 1000 g load. It can be attributed to development of built-up edges and crack formation. Figure 5a shows variation of mean indentation diagonal length with the indentation load. The indentation length increased from 5.48 to 77.45 μm with increasing indentation load from 10 to 2000 g. To further understand indentation behaviour, the SEM images of corresponding indentations at various loads of 10, 100 and 1000 g are presented in Fig. 5b. The perfect indentations without any anomaly was noticed for 10 and 100 g indentations. On the other hand, built-up edges and crack formation are noticeable for 1000 g load indentation. As mentioned above, the reduction in hardness was prominent at 1000 g load mainly due to built-up edges and crack formation as some energy spent in this process. A general observation is that the built-up edges formed for Cu–15Al at above a load of 500 g. Hence, it is meaningful to consider hardness of Cu–15Al alloy as true representative hardness below 500 g load. For example, the hardness measured at 100 g load can be even taken as bulk hardness, since the average

Figure 5 a Effect of indentation load on indentation mean diagonal length of hot-pressed Cu–15Al alloy. The SEM images of corresponding indentations at various loads of **b** 10 g, **c** 100 g and **d** 1000 g. (The hot press is carried at 500 °C, 500 MPa, 30 min under vacuum).



indentation diagonal length at 100 g load (~ 16.5 μm) covers large area of sample.

Nano-indentation hardness

Figure 6a shows the SEM image of nano-indentations obtained on Cu–15 wt% Al alloy (hot pressed at 500 MPa) having indentation spacing of 40 μm. The indentation response and mechanical properties can be evaluated from the load versus penetration depth measurements, performed at a peak load of 20 mN, using the nano-indenter tester. According to Sneddon’s equation (Eq. 1), load (*P*) applied by the indenter on the sample surface is proportional to displacement (*h*), where *α* and *m* are the indenter geometric constants. The nanohardness of the Cu–15Al was calculated using the Oliver–Pharr analysis [37, [38] which is given in Eq. (2). Where *P*_{max} represents the maximum load applied by the indenter and *A* is the indentation area. (*P*_{max} represents the maximum load applied by the indenter, *A* is the indentation area and the value of shape constant for Berkovich tip, *β* is 1.034). Since the stiffness of non-rigid indentors was considered to be effective,

reduced modulus (*E_r*) was used to calculate the elastic modulus of Cu–Al from Eq. (3), where *dp/dh* is the indenter stiffness and *A* is the projected area of elastic contact. The elastic modulus (*E_s*) of Cu–15Al sample was calculated by the reduced modulus (*E_r*) values obtained directly from the nano-indentation system using Eq. (4), where the Poisson’s ratio (*ν_s*) of the Cu–Al alloys is taken to be 0.3, indenter elastic modulus (*E_i*) is 1141 GPa and Poisson’s ratio (*ν_i*) of indenter is 0.07 [39].

$$P = \alpha h^m \tag{1}$$

$$H = \frac{P_{max}}{A} \tag{2}$$

$$E_r = \frac{dp}{dh} \left(\frac{1}{2\beta} \sqrt{\frac{\pi}{A}} \right) \tag{3}$$

$$\frac{1}{E_r} = \frac{(1 - \nu_s^2)}{E_s} + \frac{(1 - \nu_i^2)}{E_i} \tag{4}$$

A schematic of a typical load–depth curve for Cu–15 Al is presented in Fig. 6b. The area under the unloading curve represents the elastic recoverable work (*W_e*), and the area between loading–unloading curves represents the residual plastic work (*W_p*).

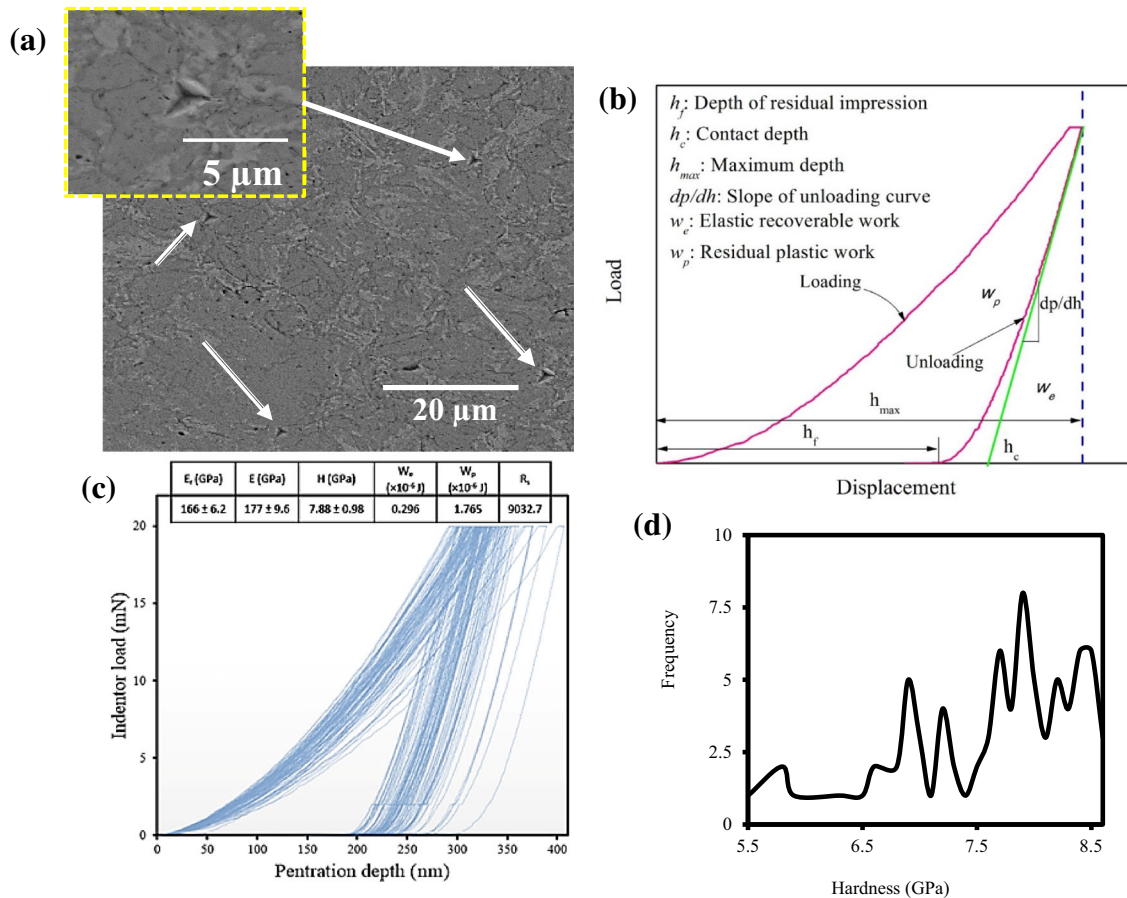


Figure 6 **a** SEM image showing typical nano-indentations obtained on hot-pressed Cu–15 wt% Al alloy having indentation spacing 40 μm . **b** Schematic of loading and unloading cycle of nano-indentation tested sample. **c** Indentation load versus penetration depth curves of Cu–15Al at an indent peak load of 20 mN (loading

and unloading rate: 2.0 mNs^{-1}). The extracted data (average values) from the plot is superimposed on the figure. Where E_r is reduced modulus, E is elastic modulus, H is hardness, W_e is elastic recovered work, W_p is residual plastic work, R_s is recovery resistance. **d** Distribution of nanohardness of Cu–15wt% Al alloy.

Where h_f is the depth of residual impression after unloading, h_c is the contact depth under the indenter and the maximum depth (h_{max}) is the total deformation corresponding to peak load at the end of loading curve. Other parameters such as plasticity index (ψ) and elasticity index can also be evaluated from the load–depth curve [40].

After completion of unloading cycle, the residual indentation depths were correlated with the measured hardness of Cu–15Al; the hardness decreases as the contact depth increases and vice versa. Similar kind of phenomena was observed in Swadener and co-workers work [41]. They also studied the effect of various shapes of indenters on hardness. From Fig. 6c, it can be observed that the maximum average displacement (h_{max}) of Cu–15 wt% Al

alloy $\sim 324 \pm 18$ nm and the average hardness (H) was found to be 7.88 ± 0.98 GPa. Further, from the unloading portion of the load–depth curves the experimentally reduced modulus (E_r) and elastic modulus (E) values were calculated to be 166.58 ± 6.2 and 177.35 ± 9.6 GPa, respectively. In the literature, it has been reported that Cu alloys such as cryogenic-treated Cu–11.76Al alloys have H of 3.67 GPa and E of 115.35 GPa [35]. In case of electro-polished Cu–11.2Al–6.9Fe alloys, maximum H of 4.9 GPa and E of 121.7 GPa was measured [42]; spray-coated Cu–17Al–1Fe alloys exhibited H of 3.35 GPa [43] and as-casted Cu–22.04 at.% Al alloys reportedly exhibited H of 3.96 GPa and E of 113.3 GPa [44]. These observations clearly indicate that the hot-pressed Cu–15 Al alloy is exhibiting superior hardness and elastic

modulus when compared to various other Cu alloys. Table 1 specifically compares nano-indentation indenter geometry and test conditions of the literature with the present work. Most of the cases Berkovich indenter and constant load test conditions were used. The indentation load (20 mN) that is used in the present work is much higher than the literature (1 mN). Since load is higher, the present experimental conditions are expected to provide better representative data.

The resistance of the Cu–Al alloy surface against plastic deformation can be given by the ratio H^3/E^2 . Where H and E are the hardness and elastic modulus, respectively. The value of H^3/E^2 for Cu–15Al is 31.45×10^3 which is directly proportional to the recovered elastic work during unloading of the indenter. From the load versus indenter penetration depth curves, the residual plastic work (W_p) and recovered elastic work (W_e) can be measured by integrating the area under unloading curve and the area between loading–unloading curves, respectively [45]. These calculations were done by using the origin® software; the recovered elastic work was measured to be 0.296×10^{-6} J and the residual plastic work (1.765×10^{-6} J). The total work can be calculated from Eq. (5).

$$W_t = W_e + W_p \tag{5}$$

The elastic–plastic or viscoelastic response of the materials under load can be described by plasticity index [40, 46]. The plasticity index (ψ) of the Cu–Al can be estimated from Eq. (6).

$$\psi = \frac{W_p}{W_t} \tag{6}$$

Generally, for ideal plastic materials, the plasticity index is considered as unity ($\psi = 1$), whereas for

ideal elastic materials the plasticity index is zero ($\psi = 0$). The plasticity index (ψ) of 0.66 was estimated for Cu–Al, which shows moderate plastic behaviour under nano-indentation test. The plasticity index (ψ) of the Cu–15Al value indicates the reduction in residual depth which is well correlated with the experimental hardness values. The elastic–plastic behaviour of the materials also can be correlated with the parameter called recovery resistance (R_s). It indicates the energy dissipation during loading and unloading cycle under nano-indentation test can be evaluated by using Eq. (7).

$$R_s = \frac{2.263 \times (E_{eff}^2)}{H} \tag{7}$$

The recovery resistance parameter (R_s) of 9032.76 for Cu–15Al under nano-indentation test, which is considered to be reasonable elastic behaviour. Similar work from the previous studies of Bao et al. [47] reported the recovery resistance (R_s) of 1108.2 for fused silica with corresponding average values of hardness (H) and elastic modulus (E) of 9.6 and 68.9 GPa, respectively. From these results, it can be estimated that the hardness (H) and elastic modulus (E) are inversely related to the recovery resistance (R_s). Also, with the decrease in elastic recovery work, the recovery resistance (R_s) increases. Figure 6d shows distribution of nanohardness plotted from load versus penetration depth curves, where the same indentations were repeated 100 times in a different location on the sample surface. The hardness distribution of Cu alloy shows the pop-in effect that is associated with phase variations. The cumulative hardness distribution spreaded over the range from 5.5 to 8.5 GPa.

Table 1 Nano-indentation test conditions and results of various Cu-based alloys

S. no.	Alloy composition	Type of indenter	Load (mN)	Loading rate (mN/s)	Hardness, H (Gpa)	Elastic modulus, E (Gpa)	Ref.
1	Cu–15Al	Berkovich	20	2	7.88 ± 0.98	177.35 ± 9.60	Present work
2	Cu–11.76Al	Berkovich	1	0.1	3.67	115.35	[35]
3	Cu–11.2Al–6.9Fe	Berkovich	(Constant depth, 500 nm)	–	4.90	121.70	[42]
4	Cu–17Al–1Fe	Vickers	–	–	1.48	–	[43]
5	Cu–22.04Al	Berkovich	1	0.1	3.96	113.30	[44]

Compression properties

A representative stress–strain curve of Cu–Al alloy after compression test is shown in Fig. 7a. The Cu–15Al measured with maximum yield strength of 985 ± 113 MPa and compressive strength of 1072 ± 74 MPa with reasonable amount of strain ($6.6 \pm 1\%$). The moderate strains produced in the Cu–15Al alloy can be a result of the presence of considerable amount of elastic recovery work (W_e) and high residual plastic work, which can be

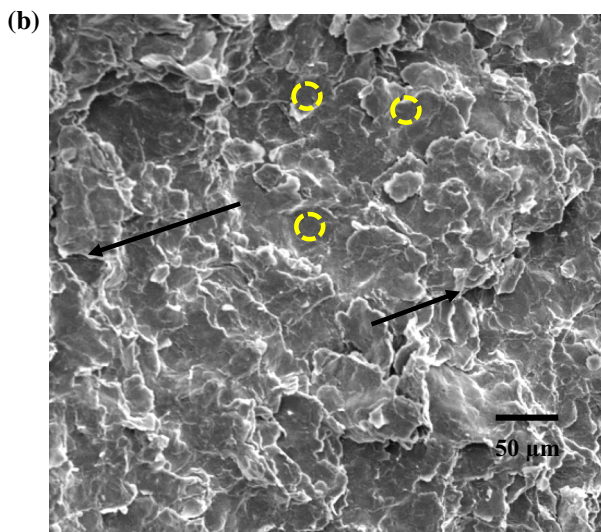
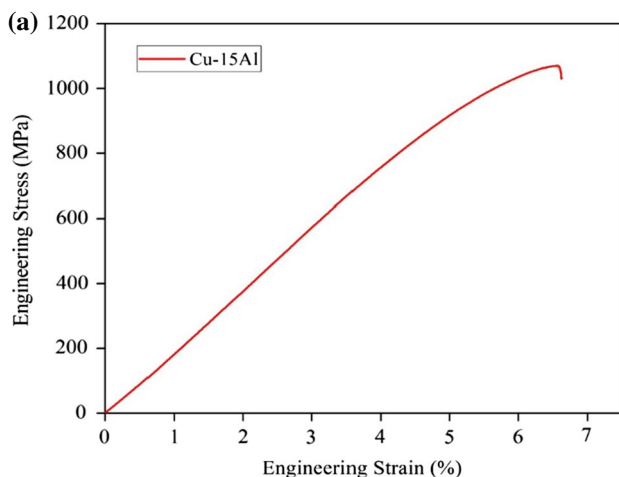


Figure 7 **a** A Representative engineering stress–strain curve (compression test) of hot-pressed Cu–15 Al alloy and **b** fractured surface of the Cu alloy after compression test showing the mixed mode of fracture. The intergranular regions are indicated with an arrow, and transgranular regions are indicated by a circle. (Hot-pressing conditions: temperature: 500 °C, pressure: 500 MPa, time: 30 min under vacuum environment).

correlated with the nano-indentation test results. The fracture surface after compression test reveals the mixed mode of fracture (Fig. 7b), and it is having more roughness indicating large energy spent during fracture.

Glass processed Cu–15Al alloy by melt-casting route at a relatively high temperature of 1150 °C and it exhibited a maximum yield strength of 720 MPa and compressive strength of 1450 MPa with a very minute strain of 0.2% [36]. In another work, Cu–14Al–2Fe-cast alloys were reported with a compressive strength of 1015 MPa and it is significantly reduced to 875 MPa when the alloy was heat treated [48]. A moderate yield strength of 650 MPa and maximum compressive strength of 1300 MPa with 24% strain were reported for Cu–10%Al–5%Ni–5%Fe alloy [49]. Nassef et al. [8] reported that the compression strength varied between 191 and 230 MPa and strain 10–16% for hot-pressed Cu–(X wt%) Sn alloys (where X = 5, 10 and 15). These observations clearly indicate that processing conditions and alloy composition have a significant effect on the compression properties of Cu alloys. Overall the Cu–15Al alloys which were developed in the present work are exhibiting a good combination of strength and hardness properties.

Wear properties

The coefficient of friction (COF) of Cu–15Al alloy as a function of sliding distance is plotted in Fig. 8. A common observation is that COF of all the samples is almost constant with the sliding distance. The slight fluctuations of COF curves can be attributed to constant formation and displacement of wear debris during the test. The wear debris characteristics will be discussed in the following. It can be observed that the COF of Cu–15 Al sample (hot pressed at 100 MPa) is relatively high when compared to other samples. Since this sample is relatively less densified, relatively more wear debris formation or surface damage would have led to increase in COF. By closely looking at Fig. 8a, b, it can be noticed that the COF samples increased with increasing sliding velocity. The average COF of Cu–15Al alloy varied between 0.15 and 0.21 at sliding velocity of 0.25 m/s, and it increased to 0.20–0.28 with further increasing sliding speed (1.5 m s^{-1}) (see Table 2). Overall, the sample that was hot pressed at 500 MPa measured with the lowest COF among all the samples. With

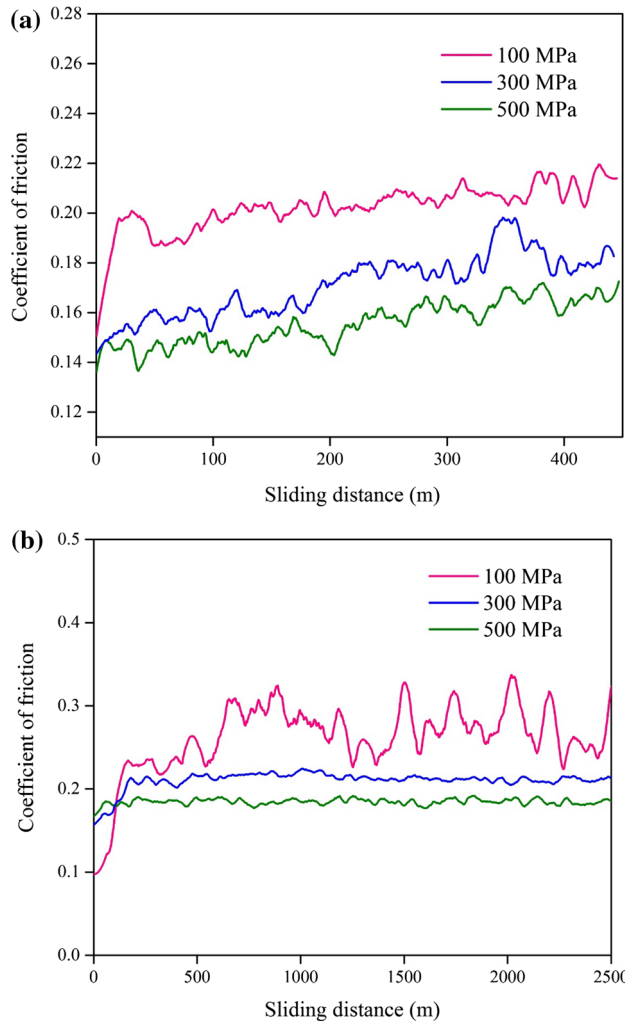


Figure 8 Coefficient of friction of Cu–15Al alloys (hot-pressed at different pressures) after sliding against SS disc at **a** sliding velocity of 0.25 ms⁻¹ and **b** sliding velocity of 1.5 ms⁻¹.

increasing sliding velocity, the weight loss of the samples also increased (see Table 2). Depending on the sliding velocity, the weight loss of Cu–Al varied between 1.15 and 15.7 mg. The weight loss of the alloy decreased with increasing hot press pressure. The wear volume of Cu–15Al is calculated using Eq. (8), and the specific wear rate of samples is calculated using Eq. (9), where *A* is cross-sectional area of the pin sample, *h* is material removal height during sliding, *L* is load applied on pin and *d* is the sliding distance.

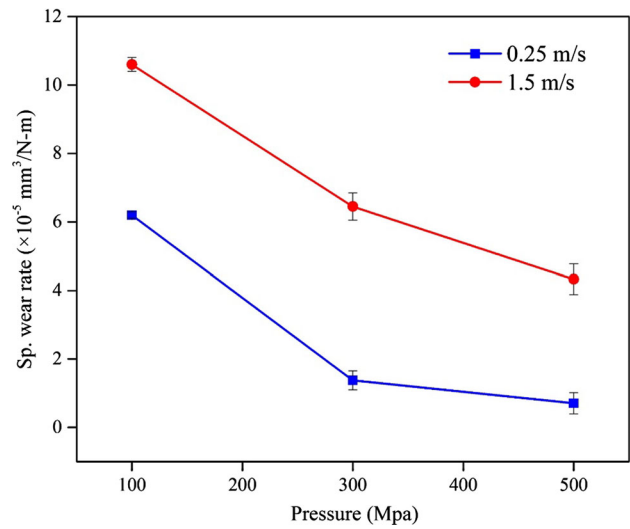


Figure 9 Specific wear rates of the Cu–15Al alloys (hot pressed at different pressures) with different sliding speeds at an applied load of 9.81 N.

Table 2 Wear properties of Cu–15Al alloys (processing conditions: 500 °C for 30 min). sliding against SS disc at a load of 9.81 N

S. No.	Alloy	Hot-pressing pressure (MPa)	Hardness, Hv (GPa)	Wear test sliding velocity (ms ⁻¹)	COF (counter body: SS)	Mass loss (mg)	Wear volume (× 10 ⁻⁹ m ³)	Sp. wear rate (× 10 ⁻⁵ mm ³ N ⁻¹ m ⁻¹)
1	Cu–15Al	100	2.10 ± 0.06	0.25	0.20 ± 0.21	9.15 ± 0.10	1.52 ± 0.02	6.20 ± 0.10
2	Cu–15Al	300	5.44 ± 0.11	0.25	0.16 ± 0.16	2.15 ± 0.50	0.33 ± 0.07	1.38 ± 0.28
3	Cu–15Al	500	6.16 ± 0.16	0.25	0.14 ± 0.15	1.15 ± 0.10	0.17 ± 0.01	0.71 ± 0.31
4	Cu–15Al	100	2.10 ± 0.06	1.5	0.27 ± 0.01	15.7 ± 0.40	2.60 ± 0.06	10.63 ± 0.20
5	Cu–15Al	300	5.44 ± 0.11	1.5	0.22 ± 0.01	10.05 ± 0.10	1.57 ± 0.01	6.43 ± 0.04
6	Cu–15Al	500	6.16 ± 0.16	1.5	0.20 ± 0.01	6.95 ± 0.10	1.05 ± 0.01	4.33 ± 0.45

$$\text{Wear volume} = \frac{\text{Weight loss}}{\text{Pin density}} \quad (8)$$

$$w = \left(\frac{A \times h}{L \times d} \right) \quad (9)$$

The wear volume increased significantly with increasing sliding speed or lowering of hot press pressure of samples. The average wear volume of Cu–15Al alloy observed to vary between 0.17×10^{-9} and $1.52 \times 10^{-9} \text{ m}^3$ at sliding velocity of 0.25 m/s and it further increased to 1.05×10^{-9} – $2.60 \times 10^{-9} \text{ m}^3$ with increasing sliding speed up to 1.50 m/s. Figure 9 shows that the specific wear rate of Cu–Al decreased with increasing hot press pressure. Nevertheless, the wear rate is significantly high for Cu–15Al that is tested at 1.5 m/s when compared to 0.25 m/s. From Table 2, it is evident that the Cu–15Al

hot pressed at 100 MPa exhibited higher wear rate ($6.20 \times 10^{-5} \text{ mm}^3 \text{ N}^{-1} \text{ m}^{-1}$ at 0.25 m s^{-1} and $10.63 \times 10^{-5} \text{ mm}^3 \text{ N}^{-1} \text{ m}^{-1}$ at 1.50 m s^{-1}) and Cu–15Al hot pressed at 500 MPa exhibited lower wear rate ($0.71 \times 10^{-5} \text{ mm}^3 \text{ N}^{-1} \text{ m}^{-1}$ at 0.25 m/s and $4.33 \times 10^{-5} \text{ mm}^3/\text{Nm}$ at 1.50 m s^{-1}). At higher sliding velocity, the wear rate of Cu–Al alloys hot pressed at 300 and 500 MPa is comparable. From this it is evident the samples that possess better density and hardness are exhibiting relatively better wear resistance under the present experimental conditions.

To understand the wear mechanisms, as a representative the morphology of worn surfaces of Cu–15Al sample (hot pressed at 500 MPa) after sliding against stainless steel disc is shown in Fig. 10. The worn surface of Cu–15Al samples reveals the grooved line features and represents abrasion wear

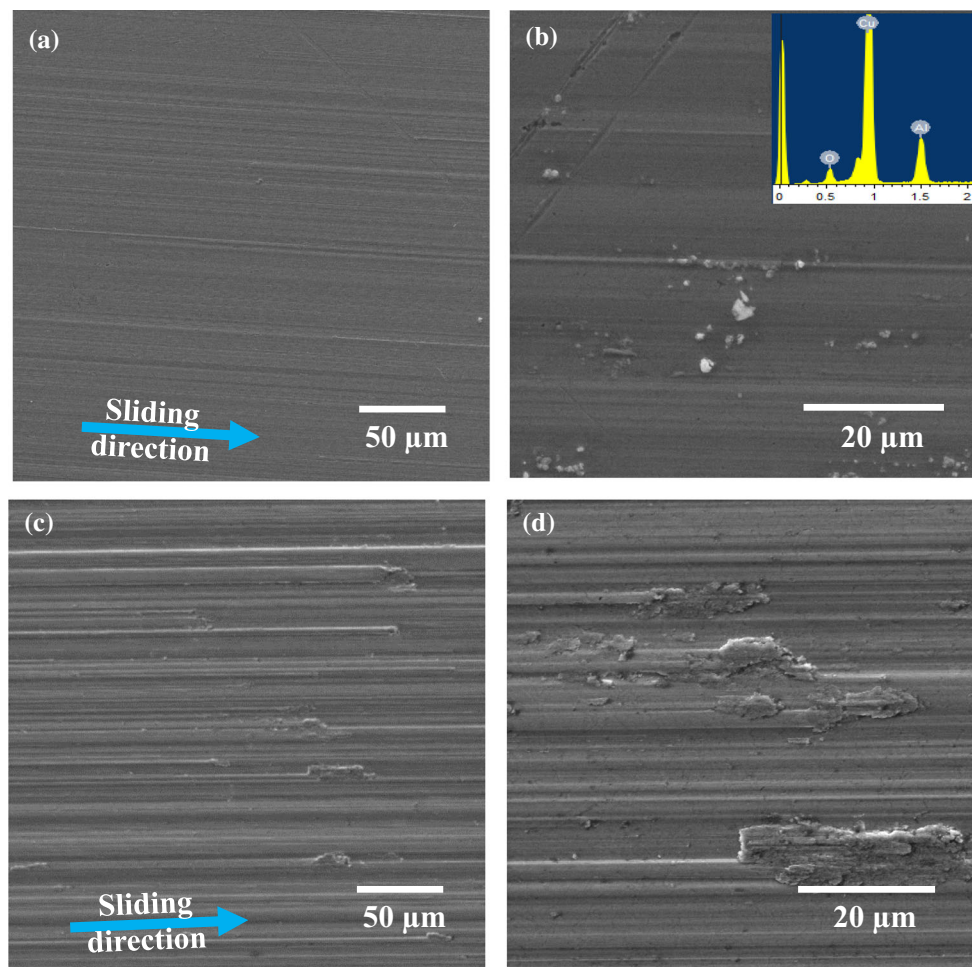


Figure 10 SEM micrographs of worn surfaces of the Cu–15Al (hot-pressing conditions: 500 °C, 500 MPa, 30 min.) alloys sliding against stainless steel disc at an applied load of 9.81 N. **a**,

b sliding velocity of 0.25 ms^{-1} ; **c**, **d** sliding velocity of 1.5 ms^{-1} . The images **b** and **d** are taken at higher magnifications.

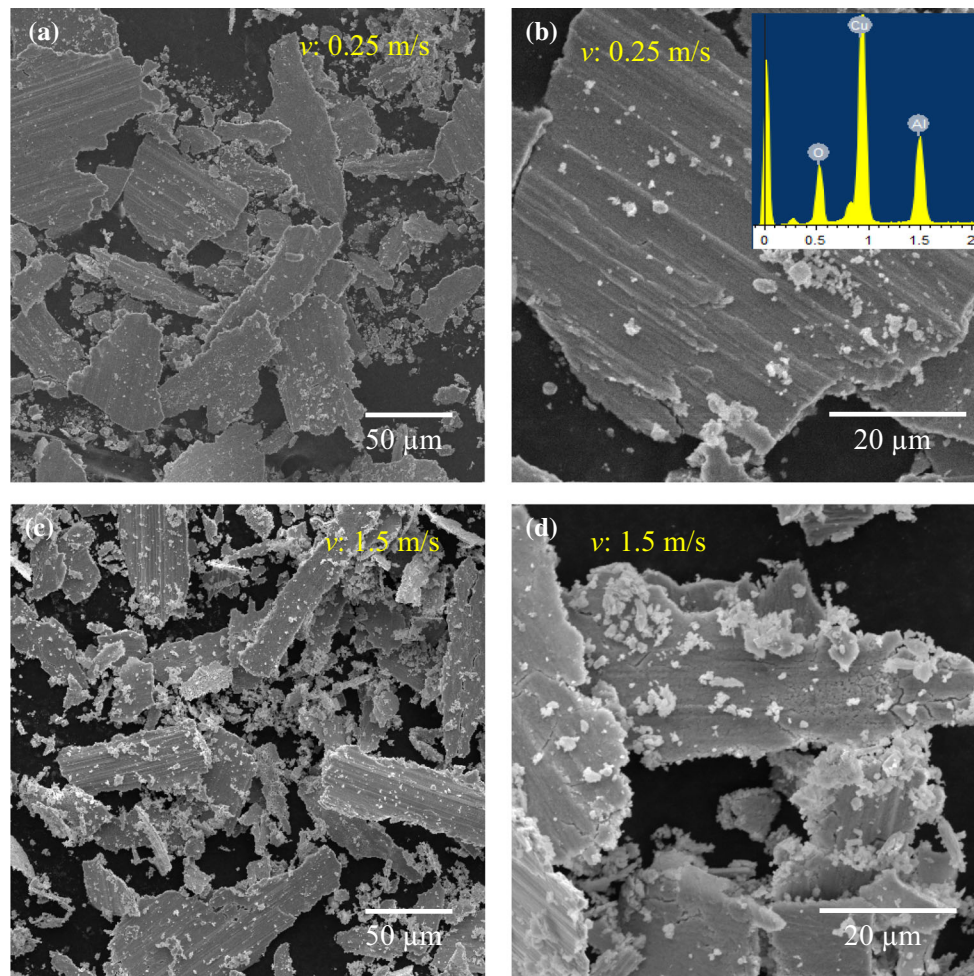


Figure 11 Surface morphology of the wear debris of the Cu–15Al alloys (processed at a pressure of 500 MPa) after wear against stainless steel disc at different sliding velocities of 0.25 m s^{-1} (a,

b) and 1.5 m s^{-1} (c, d). Large wear debris generated at a sliding velocity of 0.25 m s^{-1} compared to a sliding velocity of 1.5 m s^{-1} during wear test.

as major dominant wear mechanism. The presence of wear debris on the worn surface also can be seen in Fig. 10b. At higher sliding velocity (1.50 m s^{-1}), the worn surface is characterized with much deeper abrasion grooves and more damaged surface when compared with the worn surface that was subjected to wear test at lower velocity of 0.25 m s^{-1} (see Fig. 10a–d). The SEM–EDS elemental analysis of worn surface reveals the presence of small amount of oxygen along with Cu and Al (Fig. 10b). It indicates the formation of oxides on worn surfaces of pin as result of generation of heat during sliding against SS disc. However, XRD of worn surfaces did not provide any evidence of formation of new phase with in its detection limit. There is also no material transfer from SS disc counter body to Cu–15Al pin, since no trace of Fe etc. could not be observed from EDS spectra.

The morphology of wear debris formed during wear and its elemental analysis is presented in Fig. 11. Wear debris consist of both large and fine flakes with the size of several nanometres to $150 \mu\text{m}$. The surface of large wear debris was observed to be characterized with the presence of abrasive grooves and microcracks (Fig. 11b, d), which can be developed due to wear. In particular, the wear debris size is relatively larger at lower sliding velocity when compared to higher sliding velocity (see Fig. 11a, c). The SEM–EDS elemental analysis reveals the presence of oxygen along with Cu and Al on wear debris (Fig. 11b). A careful look at SEM–EDS of worn surface and wear debris indicates that the peak intensity of oxygen for wear debris is relatively high when compared to worn surface. The surface roughness of Cu–15Al before and after the wear test measured on

Figure 12 **a** Surface roughness profile of polished Cu–15Al sample before and after wear test. The surface roughness was measured from the two dimensional cross-sectional profile, and **b** wear tracks of alloy after a sliding distance of 2.5 km.

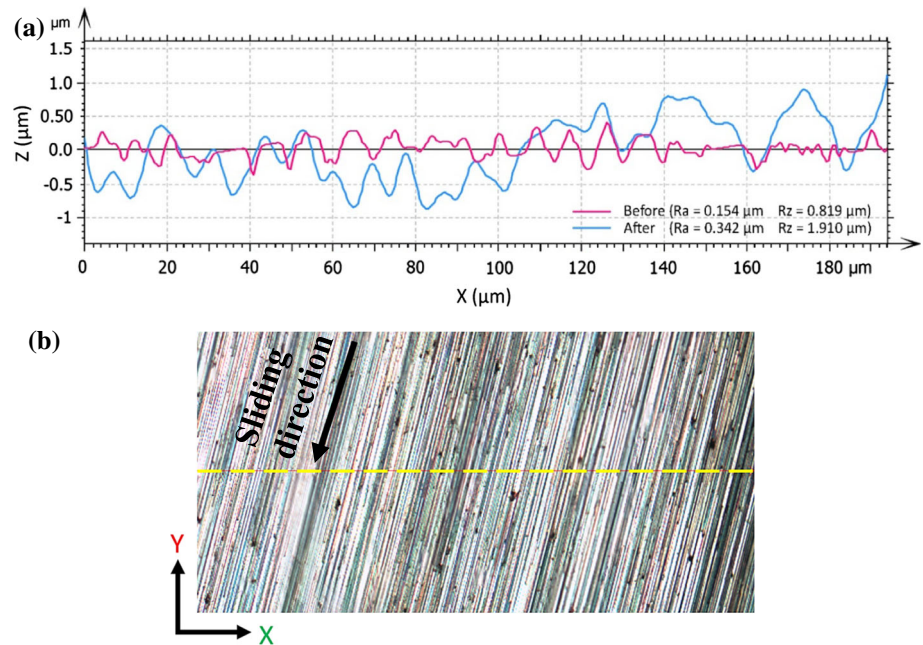


Table 3 Comparison of hardness and wear properties of Cu-based alloys (from literature) processed by various techniques

S. No.	Alloy	Process	Test conditions	Hardness, Hv (GPa)	COF (counter body: SS)	Sp. wear rate ($\times 10^{-5} \text{ mm}^3 \text{ N}^{-1} \text{ m}^{-1}$)	Ref.
1	Cu	Casting	p : 3–64, v : 0.35	0.80–1.40	0.10	26.50	[50]
2	Cu–10at.%Ag–10at.%W	PM	l : 9.81, v : 0.25	3.61	0.55	5.80	[51]
3	Cu–10at.%Ag	PM	p : 1.38, v : 0.25	5.20	0.57	23.30	[24]
4	Cu–10at.%W	PM	l : 9.81, v : 0.25	3.71	0.43	11.00	[52]
5	Cu–(0.35–0.5)Sn	Casting	l : 50–110, v : 0.1	–	0.27–0.31	0.50–3.50	[53]
6	Cu–(0.08–0.12)Ag	Casting	l : 50–110, v : 0.1	–	0.28–0.29	0.80–3.25	[53]
7	Cu–(0.3–0.5)Mg	Casting	l : 50–110, v : 0.1	–	0.29–0.32	2.80–3.75	[53]
8	Cu–(0.35–0.5)Sn	Casting	l : 80, v : 0.2	–	0.27	3.85	[53]
9	Cu–(0.08–0.12)Ag	Casting	l : 80, v : 0.2	–	0.30	8.55	[53]
10	Cu–(0.3–0.5)Mg	Casting	l : 80, v : 0.2	–	0.29	4.40	[53]
11	Cu–(5–20)W	PM	Amp: 100, l : 2–10, f : 5	1.08–1.36	0.50–0.92	8.80–9.50	[54]
12	Cu–2.2Al	Induction melting	Amp: 500, l : 20–30, f : 5–10	0.72	0.75 (Wc–Co)	6.40–10.50	[55]
13	Cu–0.8Cr–0.08Zr	Casting	l : 5–10, v : 0.2	0.93	–	WV: 6.50 mg over 2 km	[56]
14	Cu– x TiB ₂ (x : 0–2.5)	Induction melting	l : 60, v : 0.089–0.445	0.60–1.20	–	750–5200	[57]
15	Cu–10TiB ₂	SPS	Amp: 100, l : 10, f : 8	1.50–1.96	~ 0.65	150–380	[58]
16	Cu–5Pb	Stir casting	l : 40, v : 1.0	0.47	–	0.52–1.05	[59]
17	Cu–40Pb	Stir casting	l : 40, v : 1.0	0.26	–	0.12–0.56	[59]

PM powder metallurgy, SPS spark plasma sintering, l load (N), p pressure (MPa), v sliding velocity (ms^{-1}), f frequency (Hz), Amp amplitude (μm)

2D surface profile along the dotted line is presented in Fig. 12a, b. The surface roughness (R_a) of $0.15 \mu\text{m}$ was measured for the polished surface with maximum depth of roughness (R_z) of $0.82 \mu\text{m}$. The worn surface displays the height variations of the ridges and roots of wear track. Significant increase in roughness ($R_a \sim 0.34 \mu\text{m}$, $R_z \sim 1.91 \mu\text{m}$) was observed for worn surfaces of Cu–15 Al.

Hardness and wear properties of different Cu materials are presented in Table 3. Overall, the hot-pressed Cu–15Al alloy showed low specific wear rate or better wear resistance ($0.71 \times 10^{-5} \text{mm}^3 \text{N}^{-1}\text{m}^{-1}$ at 0.25m s^{-1} and $4.33 \times 10^{-5} \text{mm}^3 \text{N}^{-1}\text{m}^{-1}$ at 1.50m s^{-1}) when compared to other copper-based alloys such as Cu–Sn, Cu–Ag and Cu–Mg which were processed by casting route [45–59]. Pure Cu is reported with considerably higher wear rate of $26.5 \times 10^{-5} \text{mm}^3/\text{N}\cdot\text{m}$ [50]. On the contrary, the specific wear rate and COF of Cu–10at.%Ag–10at.%W alloy were reported to be $5.8 \times 10^{-5} \text{mm}^3/\text{N}\cdot\text{m}$ and 0.55, respectively [51]. In another work, Cu–10at.%W alloy exhibited wear rate of $11 \times 10^{-5} \text{mm}^3/\text{N}\cdot\text{m}$ and COF of 0.43 [52]. Cu–10at.%Ag alloy exhibited high wear rate of $23.3 \times 10^{-5} \text{mm}^3/\text{N}\cdot\text{m}$ and COF of 0.57 despite its high hardness [24]. It is interesting to note that Cu–Pb alloys [59] reported with better wear resistance despite its low hardness or use of severe wear testing conditions (see Table 3). Such better wear resistance of these alloys can be attributed as lubrication property of lead and its presence reduces wear of Cu [59]. Similarly, Ren et al. [24] also revealed that the hardness of the Cu alloys decreased with coarser Ag precipitates; however, these alloys exhibited superior wear resistance (by a factor of 2–20) when compared to other highly hard Cu–Ag alloys with finer precipitates. Such behaviour was related to its ability of Ag-rich nanolayers formation at sliding contact. From this, it can be inferred that high hardness may not always result in good wear resistance of materials. It majorly depends on the operative wear mechanisms.

Conclusions

- A maximum density of 94.5% pth and Vickers hardness of $\sim 6.2 \text{GPa}$ were measured for Cu–15Al alloy after hot pressing the alloy at a temperature of $500 \text{ }^\circ\text{C}$ under 500MPa pressure for 30 min.
- The XRD, SEM–EDS analysis concurrently revealed the presence of α ($\text{Cu}_{0.78}\text{Al}_{0.22}$) and γ (Cu_9Al_4) phases in the sintered samples.
- The average nano-indentation hardness of $7.88 \pm 0.98 \text{GPa}$ was measured for Cu–15 Al alloy and is the highest ever reported for this class of materials. So far in the literature, a maximum hardness of 4.9GPa was reported for Cu-based materials.
- The alloy was measured with a moderately high compressive yield strength of $985 \pm 113 \text{MPa}$, the compression strength of $1072 \pm 74 \text{MPa}$, and strain of $6.6 \pm 1\%$.
- The wear tests revealed that the Cu–15 Al alloy hot pressed at 500MPa pressure exhibited better wear properties. Low coefficient of friction (COF) of 0.15 and wear rate of $0.71 \times 10^{-5} \text{mm}^3/\text{N}\cdot\text{m}$ were observed at a sliding speed of 0.25m/s and high COF of 0.20 and wear rate of $4.33 \times 10^{-5} \text{mm}^3/\text{N}\cdot\text{m}$ noted with further increasing the sliding speed (1.25m/s). Further characterization of worn surfaces reveals abrasion wear as major dominant wear mechanism.
- The SEM–EDS elemental analysis reveals the presence of oxygen along with Cu and Al on wear debris as well as on worn surfaces of the pin. It indicates the formation of oxides on worn surfaces of pin as result of generation of heat during sliding against SS disc.
- In view of the excellent hardness, good wear and compressive strength properties of Cu–15Al alloy, it is expected to be a promising material for heavy-duty wear resistance applications such as friction welding or EDM machining electrodes.
- This work implicates that use of high hot pressure can be advantageous in densifying materials relatively at very low sintering temperatures with a good combination of properties. Hence, such process can be useful to develop ultra- or nanostructured bulk materials economically.

Acknowledgements

Ministry of Human Resource and Development, Government of India is gratefully acknowledged for the financial support to procure hot press equipment under plan grants. The authors gratefully thank the reviewers for useful comments.

References

- [1] Krebs S, Gartner F, Klassen T (2015) Cold spraying of Cu–Al–bronze for cavitation protection in marine environments. *J Therm Spray Technol* 24:126–135
- [2] Meyer L, Thedens M, Beyer M (2017) Incendivity of aluminium bronze in mechanical friction contacts. *J Loss Prev Process Ind* 49:947–952. <https://doi.org/10.1016/j.jlp.2017.02.003>
- [3] Gyimah GK, Huang P, Chen D (2014) Dry sliding wear studies of copper-based powder metallurgy brake materials. *J Tribol* 136:41601
- [4] Soliman HN, Habib N (2014) Effect of ageing treatment on hardness of Cu–12.5 wt% Al shape memory alloy. *Indian J Phys* 88:803–812
- [5] Prokoshkina D, Esin VA, Divinski SV (2017) Experimental evidence for anomalous grain boundary diffusion of Fe in Cu and Cu–Fe alloys. *Acta Mater* 133:240–246
- [6] Rabiee M, Mirzadeh H, Ataie A (2016) Unraveling the effects of process control agents on mechanical alloying of nanostructured Cu–Fe alloy. *J Ultrafine Grained Nanostruct Mater* 49:17–21
- [7] Heidarzadeh A, Saeid T (2016) Correlation between process parameters, grain size and hardness of friction-stir-welded Cu–Zn alloys. *Rare Met* 37:1–11
- [8] Nassef AE, Alateyah AI, El-Hadek MA, El-Garaihy WH (2017) Mechanical behavior and fracture surface characterization of liquid-phase sintered Cu–Sn powder alloys. *Adv Mater Lett* 8:717–722
- [9] Jawaharham GS, Dillon SJ, Averback RS (2017) Hardening mechanisms in irradiated Cu–W alloys. *J Mater Res* 32:3156–3164
- [10] Guo J, Rosalie J, Pippan R, Zhang Z (2017) On the phase evolution and dissolution process in Cu–Cr alloys deformed by high pressure torsion. *Scr Mater* 133:41–44
- [11] Korneva A, Straumal B, Kilmametov A et al (2016) Phase transformations in a CuCr alloy induced by high pressure torsion. *Mater Charact* 114:151–156
- [12] Gong YL, Ren SY, Zeng SD, Zhu XK (2016) Unusual hardening behaviour in heavily cryo-rolled Cu–Al–Zn alloys during annealing treatment. *Mater Sci Eng A* 659:165–171
- [13] Angelo PC, Subramanian R (2008) Powder metallurgy: science, technology and applications, Eastern ec. PHI Learning, New Delhi
- [14] Kajiwarra S (1967) Transformation from a lattice of ‘ABCBCACAB’ stacking order to f.c.c lattice by deformation. *J Phys Soc Jpn* 23:656
- [15] Arnberg L, Westman S (1978) Crystal perfection in a non-centrosymmetric alloy. Refinement and test of twinning of the γ -Cu₉Al₄ structure. *Acta Crystallogr Sect A Cryst Phys Diffr Theor Gen Crystallogr* 34:399–404
- [16] Han P, Xiao F, Zou W, Liao B (2014) Influence of hot press temperature on the microstructure and mechanical properties of 75% Cu–25% Sn alloy. *Mater Des* 53:38–42
- [17] Rojas P, Vera R, Martínez C, Villarroel M (2016) Effect of the powder metallurgy manufacture process on the electrochemical behaviour of copper, nickel and copper–nickel alloys in hydrochloric acid. *Int J Electrochem Sci* 11:4701–4711
- [18] Martínez C, Briones F, Rojas P et al (2017) Microstructure and mechanical properties of copper, nickel and ternary alloys Cu–Ni–Zr obtained by mechanical alloying and hot press. *MRS Adv* 2:2831–2836
- [19] Ramkumar KR, Sivasankaran S, Alaboodi AS (2017) Effect of alumina content on microstructures, mechanical, wear and machining behavior of Cu–10Zn nanocomposite prepared by mechanical alloying and hot-pressing. *J Alloy Compd* 709:129–141
- [20] Youssef KM, Abaza MA, Scattergood RO, Koch CC (2018) High strength, ductility, and electrical conductivity of in situ consolidated nanocrystalline Cu–1%Nb. *Mater Sci Eng A* 711:350–355. <https://doi.org/10.1016/j.msea.2017.11.060>
- [21] Rabiee M, Mirzadeh H, Ataie A (2017) Processing of Cu–Fe and Cu–Fe–SiC nanocomposites by mechanical alloying. *Adv Powder Technol* 28:1882–1887. <https://doi.org/10.1016/j.apt.2017.04.023>
- [22] Kumar A, Pradhan SK, Jayasankar K et al (2017) Structural investigations of nanocrystalline Cu–Cr–Mo alloy prepared by high-energy ball milling. *J Electron Mater* 46:1339–1347. <https://doi.org/10.1007/s11664-016-5125-x>
- [23] Chakravarty S, Sikdar K, Singh SS et al (2017) Grain size stabilization and strengthening of cryomilled nanostructured Cu 12 at.% Al alloy. *J Alloy Compd* 716:197–203. <https://doi.org/10.1016/j.jallcom.2017.05.093>
- [24] Ren F, Arshad SN, Bellon P et al (2014) Sliding wear-induced chemical nanolayering in Cu–Ag, and its implications for high wear resistance. *Acta Mater* 72:148–158. <https://doi.org/10.1016/j.actamat.2014.03.060>
- [25] Sharma AS, Biswas K, Basu B, Chakravarty D (2011) Spark plasma sintering of nanocrystalline Cu and Cu–10 wt Pct Pb alloy. *Metall Mater Trans A* 42:2072–2084
- [26] Sharma AS, Mishra N, Biswas K, Basu B (2013) Densification kinetics, phase assemblage and hardness of spark plasma sintered Cu–10 wt% TiB₂ and Cu–10 wt% TiB₂–10 wt% Pb composites. *J Mater Res* 28:1517–1528
- [27] Eze AA, Jamiru T, Sadiku ER et al (2018) Effect of titanium addition on the microstructure, electrical conductivity and mechanical properties of copper by using SPS for the preparation of Cu–Ti alloys. *J Alloy Compd* 736:163–171

- [28] Huang K, Yang Y, Qin Y et al (2015) A new densification mechanism of copper powder sintered under an electrical field. *Scr Mater* 99:85–88
- [29] Patra S, Mondal K (2014) Densification behavior of mechanically milled Cu–8 at.% Cr alloy and its mechanical and electrical properties. *Prog Nat Sci Mater Int* 24:608–622
- [30] Kumar A, Jayasankar K, Debata M, Mandal A (2015) Mechanical alloying and properties of immiscible Cu–20 wt% Mo alloy. *J Alloy Compd* 647:1040–1047
- [31] Hao H, Ye S, Yu K et al (2016) The role of alloying elements on the sintering of Cu. *J Alloy Compd* 684:91–97
- [32] Nassef A, El-Hadek M (2016) Microstructure and mechanical behavior of hot pressed Cu–Sn powder alloys. *Adv Mater Sci Eng* 53:38–42
- [33] Biswas K, Sharma AS, Basu B (2013) On the densification mechanisms and properties of Cu–Pb and Cu–Pb–TiB₂ nanocomposites densified using spark plasma sintering. *Scr Mater* 69:122–126
- [34] Prasad BK (1997) Dry sliding wear response of some bearing alloys as influenced by the nature of microconstituents and sliding conditions. *Metall Mater Trans A* 28:809–815
- [35] Wu LL, Liu L, Qi MS et al (2012) Effects of cryogenic treatment on micro-mechanical properties of a Cu–Al alloy. *Adv Mater Res Trans Tech Publ* 562:196–199
- [36] Glas F (2005) Ziehen von edelstahlblechen mit werkzeugen aus aluminium-mehrstoffbronzen. *Tribol und Schmier* 52:55–63
- [37] Oliver WC, Pharr GM (1992) An improved technique for determining hardness and elastic modulus using load and displacement sensing indentation experiments. *J Mater Res* 7:1564–1583
- [38] Kan Q, Yan W, Kang G, Sun Q (2013) Oliver–Pharr indentation method in determining elastic moduli of shape memory alloys—a phase transformable material. *J Mech Phys Sol* 61:2015–2033
- [39] Ebenstein DM, Pruitt LA (2006) Nanoindentation of biological materials. *Nano Today* 1:26–33
- [40] Shokrieh MM, Hosseinkhani MR, Naimi-Jamal MR, Tourani H (2013) Nanoindentation and nanoscratch investigations on graphene-based nanocomposites. *Polym Test* 32:45–51. <https://doi.org/10.1016/j.polymertesting.2012.09.001>
- [41] Swadener JG, George EP, Pharr GM (2002) The correlation of the indentation size effect measured with indenters of various shapes. *J Mech Phys Sol* 50:681–694
- [42] Kucita P, Wang SC, Li WS, et al (2015) Microstructure characterization of hypereutectoid aluminium bronze composite coating. In: *Journal of physics: conference series*. IOP Publishing, p 12010
- [43] Al-Athel KS, Ibrahim M, Arif AFM, Akhtar SS (2017) Effect of composition and thickness on the hardness and scratch resistance of copper and copper alloy coatings. *Arab J Sci Eng* 42:1–10
- [44] Wu L, Liu L, Liu J, Zhang R (2012) Effects of high pressure heat treatment on microstructure and micro-mechanical properties of Cu77. 96Al22.04 alloy. *Mater Trans* 53:504–507
- [45] Beegan D, Chowdhury S, Laugier MT (2005) Work of indentation methods for determining copper film hardness. *Surf Coat Technol* 192:57–63
- [46] Briscoe BJ, Fiori L, Pelillo E (1998) Nano-indentation of polymeric surfaces. *J Phys D Appl Phys* 31:2395
- [47] Bao YW, Wang W, Zhou YC (2004) Investigation of the relationship between elastic modulus and hardness based on depth-sensing indentation measurements. *Acta Mater* 52:5397–5404. <https://doi.org/10.1016/j.actamat.2004.08.002>
- [48] Li WS, Wang ZP, Lu Y et al (2006) Mechanical and tribological properties of a novel aluminum bronze material for drawing dies. *Wear* 261:155–163. <https://doi.org/10.1016/j.wear.2005.09.032>
- [49] Nigam PK, Jain P (2013) Effect of heat treatment on tensile and compression strength of nickel aluminium bronze (Cu–10%Al–5%Ni–5%Fe). *Arch Appl Sci Res* 5:224–230
- [50] Moshkovich A, Perfilyev V, Lapsker I, Rapoport L (2014) Friction, wear and plastic deformation of Cu and α/β brass under lubrication conditions. *Wear* 320:34–40. <https://doi.org/10.1016/j.wear.2014.08.016>
- [51] Zhu W, Zhao C, Kwok CT et al (2018) Effects of nanocrystalline microstructure on the dry sliding wear behavior of a Cu–10 at.% Ag–10 at.% W ternary alloy against stainless steel. *Wear* 402–403:1–10
- [52] Ren F, Zhu W, Chu K, Zhao C (2016) Tribological and corrosion behaviors of bulk Cu–W nanocomposites fabricated by mechanical alloying and warm pressing. *J Alloy Compd* 676:164–172. <https://doi.org/10.1016/j.jallcom.2016.03.141>
- [53] Gao Y, Jie JC, Zhang PC et al (2015) Wear behavior of high strength and high conductivity Cu alloys under dry sliding. *Trans Nonferrous Met Soc China* 25:2293–2300. [https://doi.org/10.1016/S1003-6326\(15\)63844-4](https://doi.org/10.1016/S1003-6326(15)63844-4)
- [54] Maji P, Dube RK, Basu B (2009) Enhancement of wear resistance of copper with tungsten addition (≤ 20 wt%) by powder metallurgy route. *J Tribol* 131:041602. <https://doi.org/10.1115/1.3204776>
- [55] Chen X, Han Z, Lu K (2014) Wear mechanism transition dominated by subsurface recrystallization structure in Cu–Al alloys. *Wear* 320:41–50. <https://doi.org/10.1016/j.wear.2014.08.010>

- [56] Purcek G, Yanar H, Saray O et al (2014) Effect of precipitation on mechanical and wear properties of ultra fine grained Cu–Cr–Zr alloy. *Wear* 311:149–158
- [57] Tu JP, Rong W, Guo SY, Yang YZ (2003) Dry sliding wear behavior of in situ Cu–TiB₂nanocomposites against medium carbon steel. *Wear* 255:832–835. [https://doi.org/10.1016/S0043-1648\(03\)00115-7](https://doi.org/10.1016/S0043-1648(03)00115-7)
- [58] Sharma AS, Mishra N, Biswas K, Basu B (2013) Fretting wear study of Cu–10wt% TiB₂ and Cu–10wt% TiB₂–10wt% Pb composites. *Wear* 306:138–148
- [59] Pathak JP, Tiwari SN (1992) On the mechanical and wear properties of copper–lead bearing alloys. *Wear* 155:37–47